University of Zurich[UZH]

Zurich Open Repository and Archive
University of Zurich
University Library
Strickhofstrasse 39
CH-8057 Zurich
www.zora.uzh.ch

Year: 2020

Anti-PD-L1 antibody direct activation of macrophages contributes to a radiation-induced abscopal response in glioblastoma

Ene, Chibawanye I ; Kreuser, Shannon A ; Jung, Miyeon ; Zhang, Huajia ; Arora, Sonali ; White Moyes, Kara ; Szulzewsky, Frank ; Barber, Jason ; Cimino, Patrick J ; Wirsching, Hans-Georg ; Patel, Anoop ; Kong, Paul ; Woodiwiss, Timothy R ; Durfy, Sharon J ; Houghton, A McGarry ; Pierce, Robert H ; Parney, Ian F ; Crane, Courtney A ; Holland, Eric C

Abstract: BACKGROUND Most glioblastoma recurrences occur near prior radiation treatment sites. Future clinical success will require achieving and optimizing an 'abscopal effect', whereby un-irradiated neoplastic cells outside treatment sites are recognized and attacked by the immune system. Radiation combined with anti-PD-L1 demonstrated modest efficacy in phase II human glioblastoma clinical trials, but the mechanism and relevance of the abscopal effect during this response remains unknown. METHODS We modified an immune-competent, genetically-driven mouse glioma model (forced PDGF expression + PTEN loss) where a portion of the tumor burden is irradiated (PDGF) and another un-irradiated luciferase expressing tumor (PDGF+Luciferase) is used as a readout of the abscopal effect following systemic anti-PD-L1 immunotherapy. We assessed relevance of tumor neoepitope during the abscopal response by inducing expression of EGFRvIII (PDGF+EGFRvIII). Statistical tests were two-sided. RESULTS Following radiation of one lesion, anti-PD-L1 immunotherapy enhanced the abscopal response to the un-irradiated lesion. In PDGF-driven gliomas without tumor neoepitope (PDGF+Luciferase, n=8), the abscopal response occurred via anti-PD-L1-driven, ERK-mediated, bone marrow-derived macrophage phagocytosis of adjacent un-irradiated tumor cells, with modest survival implications (median survival 41 days vs. radiation alone 37.5 days, P=.03). In PDGF-driven gliomas with tumor neoepitope (PDGF+EGFRvIII, n=8), anti-PD-L1-enhanced abscopal response was associated with macrophage and T-cell infiltration and increased survival benefit (median survival 36 days vs. radiation alone 28 days, P=.001). CONCLUSION Our results indicate that anti-PD-L1 immunotherapy enhances a radiation induced abscopal response via canonical T-cell activation and direct macrophage activation in glioblastoma.

DOI: https://doi.org/10.1093/neuonc/noz226

Posted at the Zurich Open Repository and Archive, University of Zurich
ZORA URL: https://doi.org/10.5167/uzh-178477
Journal Article
Accepted Version

Originally published at:
Ene, Chibawanye I; Kreuser, Shannon A; Jung, Miyeon; Zhang, Huajia; Arora, Sonali; White Moyes, Kara; Szulzewsky, Frank; Barber, Jason; Cimino, Patrick J; Wirsching, Hans-Georg; Patel, Anoop; Kong, Paul; Woodiwiss, Timothy R; Durfy, Sharon J; Houghton, A McGarry; Pierce, Robert H; Parney, Ian

F; Crane, Courtney A; Holland, Eric C (2020). Anti-PD-L1 antibody direct activation of macrophages contributes to a radiation-induced abscopal response in glioblastoma. Neuro-Oncology, 22(5):639-651. DOI: https://doi.org/10.1093/neuonc/noz226

N-O-D-19-00607R1

Anti-PD-L1 antibody direct activation of macrophages contributes to a radiation-induced abscopal response in glioblastoma

Chibawanye I. Ene[1,2], Shannon A. Kreuser[3], Miyeon Jung[4], Huajia Zhang[2], Sonali Arora[2], Kara White Moyes[3], Frank Szulzewsky[2], Jason Barber[1], Patrick J. Cimino[2,5], Hans-Georg Wirsching[2,8], Anoop Patel[1,2], Paul Kong[6], Timothy R. Woodiwiss[2], Sharon J. Durfy[1], A. McGarry Houghton[2], Robert H. Pierce[6], Ian F. Parney[4], Courtney A. Crane[1,3,7], Eric C. Holland[1,2,7,*]

[1]Department of Neurological Surgery, University of Washington, Seattle, Washington, U.S.A.
[2]Human Biology Division, Fred Hutchinson Cancer Research Center, Seattle Washington, U.S.A.
[3]Ben Towne Center for Childhood Cancer Research, Seattle Children's Research Institute, Seattle, Washington, U.S.A.
[4]Department of Neurological Surgery, Mayo Clinic, Rochester, Minnesota, U.S.A.
[5]Department of Pathology, Division of Neuropathology, University of Washington School of Medicine, Seattle, Washington, U.S.A.
[6]Experimental Histopathology, Fred Hutchinson Cancer Research Center, Seattle Washington, U.S.A.
[7]Alvord Brain Tumor Center, University of Washington, Seattle, Washington, U.S.A.
[8]Department of Neurology, University Hospital and University of Zurich, Zurich, Switzerland

[*]**Corresponding author**

Eric Holland, MD, PhD
Senior VP and Director, Division of Human Biology
Translational Cancer Research
Fred Hutchinson Cancer Research Center
1100 Fairview Ave N, C3-168
Seattle, WA 98109
(206) 667-6117
eholland@fhcrc.org

Running title: Radiation-induced abscopal response in glioblastoma

Conflict of Interest: None.

Abstract word count: 238

Manuscript word count (abstract, text, references, figure legends): 6732

Authorship:

Conceptualization: C.I.E., E.C.H.

Methodology: C.I.E., C.C., E.C.H.

Investigation: C.I.E., S.K., M.J., H.Z., P.K., T.R.W., K.W.M.

Data analysis: C.I.E., S.A., F.S., H.G.W., P.J.C., J.B.

Writing, Original draft: C.I.E, E.C.H.

Review and editing: C.I.E., P.J.C., A.P., S.J.D., C.C., E.C.H.

Funding acquisition: I.F.P, C.A.C., E.C.H.

Supervision: I.F.P. C.A.C., A.M.G., R.H.P., E.C.H.

Abstract

Background: Most glioblastoma recurrences occur near prior radiation treatment sites. Future clinical success will require achieving and optimizing an 'abscopal effect', whereby un-irradiated neoplastic cells outside treatment sites are recognized and attacked by the immune system. Radiation combined with anti-PD-L1 demonstrated modest efficacy in phase II human glioblastoma clinical trials, but the mechanism and relevance of the abscopal effect during this response remains unknown.

Methods: We modified an immune-competent, genetically-driven mouse glioma model (forced PDGF expression + PTEN loss) where a portion of the tumor burden is irradiated (PDGF) and another un-irradiated luciferase expressing tumor (PDGF+Luciferase) is used as a readout of the abscopal effect following systemic anti-PD-L1 immunotherapy. We assessed relevance of tumor neoepitope during the abscopal response by inducing expression of EGFRvIII (PDGF+EGFRvIII). Statistical tests were two-sided.

Results: Following radiation of one lesion, anti-PD-L1 immunotherapy enhanced the abscopal response to the un-irradiated lesion. In PDGF-driven gliomas without tumor neoepitope (PDGF+Luciferase, n=8), the abscopal response occurred via anti-PD-L1-driven, ERK-mediated, bone marrow-derived macrophage phagocytosis of adjacent un-irradiated tumor cells, with modest survival implications (median survival 41 days vs. radiation alone 37.5 days, P=.03). In PDGF-driven gliomas with tumor neoepitope (PDGF+EGFRvIII, n=8), anti-PD-L1-enhanced abscopal response was associated with macrophage and T-cell infiltration and increased survival benefit (median survival 36 days vs. radiation alone 28 days, P=.001).

Conclusion: Our results indicate that anti-PD-L1 immunotherapy enhances a radiation induced abscopal response via canonical T-cell activation and direct macrophage activation in glioblastoma.

Keywords: Glioblastoma; radiation; abscopal effect; macrophages; T-cells

Key Points:

1. Radiation synergizes with anti-PD-L1 immunotherapy in glioblastoma
2. Tumor neoepitope may enhance response to radiation and anti-PD-L1 immunotherapy
3. Anti-PD-L1 antibody directly activate macrophage phagocytic activity independent of T-cells

Importance of the Study:

A recent phase II clinical trial assessing the combination of radiation and anti-PD-L1 immunotherapy in glioblastoma showed a modest improvement in patient survival. The relevance of the abscopal response or impact of tumor neoepitope for susceptibility of glioblastoma to radiation and anti-PD-L1 immunotherapy remains unclear. We developed a representative RCAS/Tv-a luciferase-based glioblastoma model that allows for real-time assessment of the abscopal response following radiation of adjacent non-luciferase expressing glioblastoma. Glioblastoma with tumor neoepitope such as EGFRvIII are more susceptible to the abscopal response with significant macrophage and T-cell infiltration. In other glioblastoma without neoepitope expression, anti-PD-L1 antibodies enhances a radiation induced abscopal response through direct activation of an anti-tumor and pro-inflammatory phenotype in macrophages. Our results indicate that radiation and anti-PD-L1 induced abscopal response in glioblastoma may contribute to the modest survival benefit seen in human clinical trials.

Introduction

Glioblastoma is a highly aggressive intrinsic brain tumor that is diffusely infiltrative into the brain parenchyma.[1] Most recurrences following standard treatment (surgery, chemotherapy, radiation) occur within 2 cm of the prior treatment location.[2] Therefore, it is likely that any significant improvement in survival for glioblastoma patients will require assistance from the immune system to kill resistant/residual tumor cells outside prior treatment regions (abscopal response). During the abscopal response, radiation of specific tumors activates a systemic immune response to un-irradiated and distant tumor foci.[3] In humans and mice, this effect is potentiated by immune checkpoint inhibitors, resulting in an anti-tumor immunologic response outside the radiation field, even within the central nervous system (CNS).[4,5]

The clinical relevance of an abscopal effect on survival of patients with late stage non-small cell lung cancer (NSCLC) was previously assessed in a phase II prospective randomized clinical trial.[6] Results demonstrated that following a combination of radiation and anti-CTLA-4 immunotherapy, un-irradiated distant lesions regressed. This regression was associated with T-cell activation, resulting in a significant improvement in progression free survival (PFS, median = 7.1 vs. 3 months, P<.001) and overall survival (OS, median 20.4 vs. 3.5 months, P<.001).[6] A phase II prospective clinical trial combining radiotherapy with anti-PD-L1 immunotherapy (MEDI4736, Durvalumab) in newly diagnosed unmethylated glioblastomas demonstrated some efficacy, with median OS of 15.1 months versus a historical median OS of 12.7 months for new unmethylated glioblastoma.[7] Although a phase III clinical trial is necessary to confirm these findings, it suggests that the combination of radiation and anti-PD-L1 immunotherapy may enhance an immunological response to glioblastoma. It remains unclear whether,

similar to NSCLC, the abscopal response contributes to this effect on survival. It is also unclear which tumor-specific factors, such as neoepitopes or peripheral immunosuppressive mechanisms, may influence susceptibility to this treatment combination. Further, it remains uncertain what strategies could optimize the abscopal phenomenon for glioblastoma following radiation and anti-PD-L1 therapy.

In the current study, we leverage the RCAS/Tva mouse model system to study factors influencing susceptibility to the abscopal response in the setting of standard targeted radiation combined with anti-PD-L1 immunotherapy.

Materials and methods

A detailed description of the Methods can be found in the Supplementary Methods (available online). All animal experiments were done in accordance with guidelines from the Institutional Animal Care and Use Committee, Fred Hutchinson Cancer Research Center (IAUCUC Protocol #50842).

Mouse models of glioblastoma

The RCAS/Tva model system was used to generate mouse glioblastoma.[8,9] The 1) Tg(*NTva*); *Cdkn2a (Ink4a-Arf)*$^{-/-}$*; Pten*$^{flox/flox}$ (referred to as *NTva*), Tg(*NTva*); *Cdkn2a (Ink4a-Arf)*$^{-/-}$*; Pten*^{floxlflox}; *LSL Luciferase* and EGFRvIII. 2) Tg(*NTva); Cdkn2a*^{wt}*; Pten*$^{flox/flox}$*; CX3CR1*$^{+/GFP}$*; CCR2*$^{+/RFP}$ mice[10] were used as genetic backgrounds for RCAS mediated glioblastoma formation. Details of the full EGFRvIII cDNA which also encodes the unique EGFRvIII splice junction peptide or neoepitope (Peptide sequence-LEEKKGNYVVTDH) and mice strains used for conditional over-expression were previously described[11,12] and summarized in supplemental methods online. For bilateral tumor models, following introduction of RCAS-*PDGFB* with RCAS-*Cre* into one hemisphere and RCAS-*PDGFB* with

RCAS-*shPten* into the contralateral hemisphere, two genetically similar tumors develop, with one tumor lacking luciferase expression (PDGFB/shPten; radiated glioblastoma) and the other tumor demonstrating luciferase or EGFRvIII expression (un-irradiated glioblastoma).

Bilateral tumor formation *in vivo*

Bilateral tumors were generated in 4-6-week-old male and female adult mice. DF1 cell delivery was performed with a 30-gauge needle attached to a Hamilton syringe and stereotactic fixation device (Stoelting, Wood Dale, IL). Cells were injected into the frontal cortex of each hemisphere, 3mm lateral to bregma and a depth of 1mm. Mice were monitored carefully for signs of disease and treatment began when the tumor was visible by bioluminescence or magnetic resonance imaging (MRI).

Drug treatments *in vivo*

Adult mice were sedated with isoflurane during radiation. 10Gy was delivered to the right hemisphere (non-luciferase tumor) while the left hemisphere (Luciferase or EGFRvIII expressing tumor) and rest of body was shielded to prevent radiation on non-target tissue. Restricted radiation was confirmed by phosphorylated histone 2AX (pH2AX) expression in the non-radiated hemisphere two hours post treatment. Endotoxin low (≤0.001 EU/µg; ≤ 1 EU/mg) *and functional grade* rat anti-mouse $IgG_2b\kappa$ (isotype control), anti-PD-L1 and anti-PD1 (10µg/g mouse body weight) were administered starting on the day of radiation (post tumor initiation day 15) and then daily until endpoint. Bioluminescence signals were obtained for each treatment group every 2-3 days following treatment. The last bioluminescence signal represents the last time point measured prior to reaching end-point (see Kaplan-Meier curve for end-points). Animals were sacrificed upon development of neurological symptoms as defined by the Institutional Animal Care and Use Committee.

Bioluminescence and MRI

Bioluminescence imaging was obtained on the Xenogen IVIS 100 system. Mice with tumors expressing luciferase were anesthetized with isofluorane before intraperitoneal injection with 75mg/kg body weight D-luciferin (Caliper Life Sciences Part Number #119222). Ten minutes after injection, images were acquired for 3-5 mins. Total flux (photons seconds^{-1}) was obtained from each mouse. An MRI scan (Bruker 1T scanner) was obtained immediately after or just prior to bioluminescence to delineate tumor and inflammation. Mice were imaged on this combination protocol the first day of treatment and 3, 5, 10, 14 and 21 days after treatment. Volume of interest were manually contoured along the T2-hypertense rim of tumors for all animals on the *Viviquant* software (*Invicro*, Boston Massachusetts).

Standard immunohistochemistry

Mouse brains were fixed in formalin and embedded in paraffin, then sectioned at 5μm and stained by routine hematoxylin and eosin (H&E), as well as immunohistochemistry (IHC). Automated Immunohistochemistry was performed on the Discovery XT, (Ventana Medical Systems Inc.) according to the manufacturer's standard protocol.

***In vitro* fluorescent labeled bacteria phagocytosis**

Following 8 hours of serum starvation, mouse macrophages were treated with specific antibodies for 24 hours. The effect of anti-PD-L1 antibodies on macrophage phagocytosis was assessed using the Vybrant Phagocytosis Assay Kit (V-6694, Thermo Fisher).

Selective ERK1/2 Pathway inhibition

The selective ERK1/2 inhibitor PD98059 was purchased from Cell Signaling technology (#9909). For the *in vitro* studies, macrophages were serum starved for 8 hours and pre-incubated in specified concentrations of PD98059 1 hour prior to addition of anti-PD-L1 antibodies (20μg/ml). For western blot (ERK phosphorylation), cell lysates were obtained at 30 minutes and 3 hours following treatment with anti-PD-L1 antibodies. Mouse (Anti-PD-L1, BioXcell), Human (Avelumab, Merck and Atezolizumab, Genentech).

Differentiation of monocytes into macrophages *in vitro*

At least three biological replicates were used in each mouse macrophage experiment, while donor human peripheral monocyte derived macrophages were evaluated per antibody tested. To obtain enough starting mouse monocytes for macrophage differentiation, one mouse bone marrow derived macrophage biological replicate was derived from pooling bone marrow from the hind legs of four separate mice. Mouse bone marrow derived monocytes were harvested from *NTva; Ink4a/arf*$^{-/-}$*; Pten*$^{flox/flox}$ mice and differentiated into macrophages with 50μg/mL of macrophage colony stimulating factor (M-CSF) in RPMI medium with 10% fetal bovine serum (FBS) for 6 days. Mouse macrophages were re-plated at $5x10^5$ cells per well (6-well plate) and allowed to rest overnight prior to treatments. Flow cytometry for CD11b, F4/80, PD-L1 and PD-1 were performed to verify mouse bone marrow derived macrophages generated *in vitro*.

Antibody depletion of T-cells

On post-tumor initiation day 10, 15, 19, 22 and 30 tumor bearing mice were treated with 0.4mg of depleting antibodies via intraperitoneal route; rat anti-mouse $IgG_2b\kappa$ (isotype control BioXCell

BE0090), rat anti-CD4 (GK1.5 clone, BioXCell BE0003-1) and rat anti-CD8 (2.43 clone, BioXCell BE0061). Spleens (n=2) were harvested from each treatment group on post-tumor initiation day 22 and evaluated by flow cytometry for T-cell depletion using the following antibodies; CD8-PE (Biolegend 100708) and CD4-APC (Biolegend 100515).

Nanostring gene expression analysis

Conditions for Nanostring gene expression profiling were untreated and anti-PD-L1 (20μg/ml). Conditions for Real time PCR verification were isotype control (negative control), lipopolysaccharide (LPS; positive control, Sigma L3024), anti-PD-L1 (20μg/ml) and soluble rhPD-1-fc (20μg/ml). Following specified treatment for 200 minutes, media was aspirated, cells were rinsed in sterile PBS and lysed in RTL (Qiagen 1015750) + 1% BME (Biorad 161-0710) at 3,500 cells/μL per Nanostring recommendations. (PCR samples were lysed in 350μL). The mouse myeloid innate immunity panel (XT-PGX-MMV2-Myeloid, Nanostring 11500181) was used to assess the expression of immune related genes following treatment per Nanostring protocol.

Statistical analysis

Statistical analysis was performed using GraphPad prism 7 (GraphPad Software, San Diego, CA). Data were expressed as mean (SEM). Two-sided Mann-Whitney U tests were used to compare groups. In Figure 3A-D, the Holm-Bonferroni multiple comparison post hoc test was performed to compare differences between groups. For survival studies, the Kaplan-Meier analysis was performed using the Log-rank (Mantel-Cox) test. A P value <.05 was considered statistically significant.

Results

Effects of anti-PD-L1 and anti-PD-1 immunotherapy on survival of bilateral PDGF-driven glioblastoma bearing mice following unilateral radiation therapy

To visualize and optimize the abscopal response for glioblastoma *in vivo*, we generated two genetically distinct PDGF-driven glioblastomas within the brain. In one hemisphere, we induced a PDGF-shPten-driven glioblastoma, while in the other hemisphere we generated a PDGF-driven glioblastoma with Luciferase expression (Figure 1A; Ntva Ink4a/Arf$^{-/-}$ Pten$^{flox/flox}$ mice with *Lox-Stop-Lox* Luciferase) via deletion of the *Lox-STOP-Lox* sequence through injection of RCAS-Cre only in one side (Figure 1A, *top*). To evaluate the influence of specific tumor neoepitope expression during an abscopal response, we induced unilateral expression of EGFRvIII which contains the unique fusion junction peptide, LEEKKGNYVVTDH (Figure 1A; Ntva Ink4a/Arf$^{-/-}$ Pten$^{flox/flox}$ mice with *Lox-Stop-Lox* EGFRvIII) via deletion of the *Lox-STOP-Lox* sequence through injection of RCAS-Cre only in one side (Figure 1A, *bottom*). In the PDGF-Luciferase (PDGF+Luc) mice, restriction of luciferase expression to one hemisphere (the non-radiated side) allowed the unilateral bioluminescence readout of tumor cell viability following radiation of the other hemisphere. Radiation-induced damage was restricted to the radiated hemisphere as determined by phospho-histone 2A.X immunostaining two hours post radiation treatment (Supplemental Figure 1A). Post radiation tumor growth was assessed *in vivo* by two methods: 1) MRI to visualize bilateral tumor growth (Figure 1B; *left*) and 2) bioluminescence as a readout of tumor cell viability on the non-radiated hemisphere (Figure 1B; *right.* Correlation between MRI and bioluminescence, Figure 1C; R^2 =0.9649).

We then assessed how checkpoint inhibition could functionally enhance targeted immune response to un-irradiated tumor *in vivo* by determining the relative effects of systemic anti-PD-L1 and anti-PD-1 immunotherapy (either daily 10μg/g anti-PD-L1 or anti-PD-1) on survival when combined

with unilateral radiation. Administration of anti-PD-L1 immunotherapy in conjunction with unilateral radiation resulted in a modest improvement in survival in PDGF+Luc glioblastoma (n=7-8/group, median survival = 40.5 days vs. radiation alone 37.5 days, Log-rank P=.03, Figure 1D). In PDGF+EGFRvIII glioblastoma, there was increased improvement in survival following anti-PD-L1 immunotherapy and unilateral radiation (n=8/group, median survival = 36 days vs. radiation alone 28 days, Log-rank P=.001, Figure 1E). In a one-sided brain tumor model, 10Gy unilateral radiation to non-tumor brain had no effect on survival (Supplemental Figure 1B-C). This indicated that combination therapy (radiation and systemic anti-PD-L1) was superior to monotherapy (systemic anti-PD-L1 alone) in the RCAS/TV-a glioblastoma mouse model. Of note, this response occurs in the absence of significant PD-L1 expression within the PDGF+Luc or PDGF+EGFRvIII micro-environment (Supplemental Figure 2A-B for Multiplexed Immunohistochemistry).

Comparison of bioluminescence activity with brain MRI for *in vivo* measurement of tumor cell viability following combined glioblastoma therapy

To determine if the enhanced survival benefit from combined radiation and anti-PD-L1 immunotherapy is associated with reduction of tumor cell viability on the contralateral non-radiated side, we compared changes in routine MRI signal, representing tumor volume and inflammation, to luciferase activity, representing tumor viability in the PDGF+Luc model. In IgG control treated animals, an increase in un-irradiated tumor growth corresponded with increased MRI signal (n=8/8, Figure 2B). As a positive control, whole brain radiation with 10Gy caused a decrease in both MRI signal and luciferase activity (n=4/4, Figure 2B). Monotherapy with daily systemic anti-PD-L1 antibodies (10μg/g) had no impact on tumor progression based on MRI imaging or luciferase activity (n=0/4, Figure 2B). Unilateral radiation alone resulted in continued tumor growth as measured by MRI in all cases, but a

subset of these tumors concurrently showed a small but not significant decrease in viable tumor cell numbers as measured by reduced luciferase activity, indicating a potential abscopal effect for unilateral radiation alone occurring in only a few treated animals (n=2/4, Figure 2B). Conversely, concurrent daily systemic anti-PD-L1 immunotherapy enhanced this abscopal effect of 10Gy radiation on the un-irradiated, luciferase-containing tumor. This combined therapy resulted in a decrease of tumor cell viability in 8/8 mice (100%) and an increase in MRI signal in 5/8 mice (62.5%, Figure 2B; tumor cell viability or luciferase activity for all groups shown in Figure 2C). The discordance between loss of viable tumor cell and increased tumor size may represent treatment-induced inflammation (pseudoprogression) and/or edema falsely mimicking tumor progression on MRI. These results suggested that, following radiation and anti-PD-L1 immunotherapy, regression of un-irradiated lesions may contribute to improved survival in the bilateral brain tumor model.

Effect of anti-PD-L1 immunotherapy on radiation therapy-mediated recruitment of macrophages and T-cells into brain tumors

To investigate the relevance of tumor neoepitope expression during the abscopal response, we histologically quantified macrophage ($Iba1^+$) and T-cell ($CD3^+$) infiltration into tumors on both irradiated and un-irradiated sides of both glioma models (PDGF+Luc and PDGF+EGFRvIII) after treatment with radiation and anti-PD-L1 immunotherapy on post-treatment day 10. Relative to IgG isotype control (n=5), 10Gy radiation and daily anti-PD-L1 immunotherapy (n=5) induced a significant macrophage ($P<.0001$) and T-cell ($P<.0001$) infiltration into both un-irradiated and radiated sides of PDGF+EGFRvIII gliomas (Figure 3A-D, 3F). In PDGF-Luc gliomas (n=5), relative to IgG isotype control (n=5), there was an absence of T-cell infiltration ($P>.05$). However, a macrophage-predominant response was noted in both un-irradiated ($P<.0001$) and irradiated tumors ($P<.0001$), (Figure 3A-D and

3E). These results indicated that following radiation and anti-PD-L1 immunotherapy, the slightly higher survival advantage noted in the neoepitope expressing PDGF+EGFRvIII glioma bearing mice (relative to the PDGF+Luc glioma mice) may be due to an inherent ability to recruit T-cells into un-irradiated and irradiated tumors.

In PDGF+Luc gliomas (lacking tumor neoepitope), systemic depletion of circulating $CD4^+$ and $CD8^+$ T-cells did not affect the survival benefit associated with radiation combined with anti-PD-L1 immunotherapy (Figure 4 A-C). Therefore, to investigate the impact of macrophage recruitment on glioma growth independent of T-cell activation, we sought the source of tumor-infiltrating macrophages following radiation and anti-PD-L1 immunotherapy. We generated bilateral PDGF-$Pten^{-/-}$ glioblastoma (lacking tumor neoepitope) in the *NTva; Cdkn2a^{wt}; Pten$^{flox/flox}$; CX3CR1$^{+/GFP}$; CCR2$^{+/RFP}$* mouse model. Here, *CX3CR1$^{+/GFP}$* and *CCR2$^{+/RFP}$* delineate microglia (GFP^+) and peripheral monocytes (RFP^+), respectively, and double positive $CX3CR1^{+/GFP}/CCR2^{+/RFP}$ delineates peripherally derived tumor-associated macrophages (GFP^+/RFP^+).[13] Relative to radiation alone (n=6), the addition of daily anti-PD-L1 immunotherapy to unilateral 10Gy radiation (n=6) significantly increased the numbers of double positive $CX3CR1^{+/GFP}/CCR2^{+/RFP}$ circulating monocyte-derived macrophages in both un-irradiated (median increase 40%, P<.01) and radiated bilateral tumors on post-treatment day 5 (median increase 30%, P<.01), (Figure 4D and 4E; Flow cytometry gating strategy in Supplemental Figure 3A). It also demonstrated a loss of microglia (shown as a percentage of viable cells) within the radiated tumor, consistent with a known consequence of direct radiation on the tumor micro-environment.[14] Further investigation of this macrophage response showed that, similar to human glioblastoma,[15] RCAS/Tv-a glioblastoma-bearing mice demonstrated elevated levels of immunosuppressive $PD\text{-}L1^+/Ly6C^+$ monocytes in peripheral blood relative to healthy non-tumor mice (n=5 per PDGF+Luc or

PDGF+EGFRvIII healthy and tumor mice) (P<.01), (Supplemental Figure 3B; Flow cytometry gating strategy in Supplemental Figure 3C). Following a combination of radiation and anti-PD-L1 immunotherapy, flow cytometry of tumors from PDGF-*Pten*$^{-/-}$ glioblastoma in the CX3CR1$^{+/GFP}$/CCR2$^{+/RFP}$ model demonstrated that, relative to radiation alone (n=6), combining radiation with daily anti-PD-L1 immunotherapy (n=6) increased the fraction of Ly6C^{+} immune cells (shown as percentage of all viable cells) within both irradiated and un-irradiated tumors on post-treatment day 5 (P<.01), (Supplemental Figure 3D; Flow cytometry gating strategy in Supplemental Figure 3F). Further, increased levels of the PD-L1^{+}/Ly6C^{+} sub-population infiltrated the non-radiated tumor (P<.05), (Supplemental Figure 3E; Flow cytometry gating strategy in Supplemental Figure 3F). These data suggested that the combination of radiation and anti-PD-L1 immunotherapy enhanced recruitment of bone marrow derived immunosuppressive PD-L1^{+} monocytes into adjacent un-irradiated glioblastoma as tumor-associated macrophages.

Effect of anti-PD-L1 antibodies on monocyte-derived macrophage activation *in vitro*

Previous research has shown that anti-PD-1 antibody direct activation of PD-1^{+} macrophages, independent of T-cell activation, results in a pro-inflammatory, anti-tumor phenotype in tumor-associated macrophages.[16] Therefore, we investigated whether anti-PD-L1 antibodies could also directly induce an anti-tumor phenotype in bone marrow derived PD-L1^{+} macrophages *ex vivo*. Incubation of bone marrow derived M-CSF differentiated PD-L1^{+}/CD11b^{+}/F4/80^{+} macrophages (Supplemental Figure 4A; flow cytometry gating strategy in Supplemental Figure 4B) with anti-PD-L1 antibodies induced a shift in gene expression in mouse macrophages *in vitro* (Supplemental Table S1). Upregulation of 95 myeloid-related genes, and downregulation of 44 genes, was induced with anti-PD-L1 treatment (Supplemental Table S2). Most of these genes were related to increase in cell cycle and cytokine

production (Figure 5A and 5B). There was evidence of signaling associated with both activation and inhibition of macrophage function (Supplemental Table S2) indicating that subsequent macrophage phenotype is dependent on the balance between pro-inflammatory and pro-tumor gene expression or signaling pathways. Targeted myeloid-related gene expression was validated by real-time quantitative PCR (RT-qPCR) using an isotype negative control (IgG_2b), lipopolysaccharide (LPS) as positive control, Fc conjugated soluble PD-1 (sPD-1-Fc, IgG_1 isotype) and anti-PD-L1 antibody (IgG_2b isotype). Relative to isotype control, anti-PD-L1 induced significant increases in pro-inflammatory gene expression in macrophages (Olr1, Cxcl3, and Ccl3, P<.01), (Supplemental Figure 4C and Supplemental Table S3 and S4). sPD-1 was equally effective at inducing pro-inflammatory gene expression changes relative to anti-PD-L1 antibody, illustrating the on-target effects of anti-PD-L1 (P<.01), (Supplemental Figure 4C).

Effect of anti-PD-L1 antibodies on macrophage phagocytic activity via extracellular signal-related kinase (ERK) pathway activation

Gene ontology on the Nanostring gene expression data was indicative of both activation and inhibition of ERK pathway following incubation of PD-$L1^+$/PD-1^- mouse macrophages with an anti-PD-L1 antibody, with more significance in ERK activation signaling pathways (Figure 5A). To further explore this, we expanded the treatment regimen of mouse macrophages *in vitro* to include two clinical grade human anti-PD-L1 antibodies: Avelumab and Atezolizumab. All mouse and human anti-PD-L1 antibodies induced ERK phosphorylation in their respective macrophages *in vitro* (Figures 5C, 5D, 5E and 5F). This effect was not observed when PD-L1 treated macrophages were exposed to the selective ERK inhibitor PD98059 (Figures 5C, 5D, 5E and 5F). Functionally, anti-PD-L1 antibodies also significantly enhanced macrophage *in-vitro* phagocytic activity (P<.0001), (Figure 6A). This anti-PD-

L1-driven phagocytic effect was reversed by pre-treatment of the macrophages with the selective ERK inhibitor PD98059 (P<.0001) (Figure 6A). *In vivo,* following radiation and anti-PD-L1, there was also increased phagocytosis of tumor cells based on immunohistochemical colocalization of $Olig2^+$ tumor cells within $Iba1^+$ macrophages in both irradiated and un-irradiated low baseline intra-tumoral PDGF+Luc glioblastoma (P<.01), (Figure 6B and 6C). Anti-PD-L1 treatment alone did not increase phagocytosis of tumor cells *in-vivo* (*Data not shown*). This indicated that following a radiation-induced recruitment of the immunosuppressive $PD\text{-}L1^+$ monocytes to brain tumors, anti-PD-L1 antibodies directly induced a pro-inflammatory and anti-tumor phenotype in $PD\text{-}L1^+$ tumor-infiltrating macrophages, resulting in enhanced phagocytosis of tumor cells in the periphery of the prior radiation site.

Discussion

The specific mechanism mediating the abscopal phenomenon remains an enigma. Based on a metanalysis, the relative contribution of antigen-presenting cells (APCs) such as macrophages, dendritic cells or T-cells to the abscopal response varies depending on radiation schedule, dosage, animal model or immune checkpoint inhibitor used.[17] Prior to T-cell activation during the abscopal response, radiation-induced tumor death results in release of neo-antigens or neo-epitopes which are engulfed by APCs.[18] APCs then circulate to lymph nodes where neo-antigen presentation results in activation and education of naïve T-cells. Activated and tumor-specific T-cells enter the circulation and selectively target tumor cells, resulting in regression of un-irradiated tumors.

Even though the abscopal response is well known in other cancer types, the complete mechanism mediating immune recognition of untreated tumors remains an enigma.[17] Our results indicate that

glioblastomas with neoepitopes such as EGFRvIII tumors may be more susceptible to an immunological mediated abscopal response, although the functional significance of T-cell infiltration or neo-epitope type for survival is currently being investigated. A majority of glioblastoma, however, lack neo-epitope expression.[19] Therefore, uncovering strategies that enhance the immunologic response to glioblastoma in the absence of neo-epitope associated T-cell recruitment may improve survival. Direct activation of macrophages has been associated with the abscopal response in the absence of T-cell infiltration.[20-22] Given the critical role of macrophages demonstrated in the response to immunotherapy in our model, a better understanding of mechanisms that could enhance the macrophage-dependent abscopal effect is warranted. One possibility is the release of inflammatory cytokines or death associated molecular patterns (DAMPs) from dying tumor cells.[18,21,22] Following radiation induced recruitment to the brain, infiltrating macrophages are polarized by anti-PD-L1 antibodies into anti-tumor states resulting in eradication of previously viable tumor cells just outside of the irradiated area (the bystander effect). A second possibility is that macrophages are 'educated' by tumor antigens released following irradiation resulting in a tumor specific response. The mechanism behind this macrophage 'education', however, remains unknown and warrants further investigation.

Although blockade of PD-1 and PD-L1 are often thought of as equivalent, the effect of anti-PD-1 in our mouse model is not similar to anti-PD-L1. One reason for this phenotypic distinction is that anti-PD-L1 seems to directly activate PD-L1^{+} macrophages to increase production of cytokines and enhance phagocytosis in an ERK signaling-dependent manner. Since glioblastomas are enriched with macrophages (20-30% of tumor mass),[23-26] these immune cells may serve as better agents for achieving an immune-induced therapeutic effect. In some late stage cancer types, anti-PD-1 also activates phagocytosis in some tumor associated macrophages,[16] an effect dependent on expression of PD-1 by

these macrophages. In glioblastoma there is little PD-1 expression within the tumor and on circulating monocytes of tumor-bearing mice. By contrast, PD-L1 is expressed at higher levels on circulating monocytes of tumor bearing mice and human glioblastoma patients.[15] A recent report showed that anti-PD-L1 antibodies directly activate bone marrow derived macrophages *in-vitro*,[27] indicating that similar to anti-PD-1, anti-PD-L1 activated macrophages could also mediate an anti-tumor response independently of T-cell activation. Given that macrophages comprise the largest immune cell population in glioblastoma and PD-L1$^+$ circulating monocyte-derived macrophages are the cells that respond primarily to radiation therapy,[28] it is not surprising that after radiation therapy, mouse glioblastoma respond better to anti-PD-L1 therapy which specifically target infiltrating PD-L1$^+$ macrophages, than to anti-PD-1 immunotherapy.

In our model, we also found that anti-PD-L1 monotherapy treated mice had poorer survival relative to IgG control treated mice. Although it remains unclear why this occurred, it indicates that without radiation therapy, anti-PD-L1 therapy may have a unique profile of targets and consequently a different outcome in tumor bearing mice not receiving radiation therapy. Also, because patients with PD-L1-negative tumors also respond to anti-PD-L1 therapy,[29] our results indicate that levels of PD-L1$^+$ monocytes in circulation, not tumor PD-L1 expression, may be a better prognostic indicator of response to anti-PD-L1 therapy following radiation for glioblastoma patients. To the degree that the mouse model reflects human biology, our results also suggest that patients with glioblastoma that fail anti-PD-1 or anti-PD-L1 monotherapy could still respond to anti-PD-L1 combined with high-dose radiation of viable tumor cells.

Our study has several limitations. Since the gene expression profiling is based on macrophages cultured *in-vitro*, it may not represent the macrophage phenotype *in-vivo* therefore, we plan to perform gene expression analysis from tumor cells and macrophages post-treatment *in-vivo*. Also, given the limited specificity of CCR2 and CX3CR1 as immune cell markers, we also plan to perform lineage studies using fluorescence tagged bone marrow precursors to selectively track monocytes and macrophages following radiation and anti-PD-L1 therapy. The scope of genetic alterations assessed is also a limitation, therefore, we plan to assess the impact of other clinically significant mutations such as isocitrate dehydrogenase 1 (IDH1) mutation.

In summary, experimentally-tractable models with representative histology in immune-competent mouse backgrounds are needed to optimize the abscopal effect for brain tumors. Such experimental systems also need to be robust at detecting, monitoring, and studying the abscopal effect in live animals following administration of diverse immunotherapeutic agents irrespective of route of administration. Using the RCAS/Tv-a system, we find that anti-PD-L1 immunotherapy enhances a radiation therapy induced abscopal response. In tumors such as glioblastoma, where recurrence is driven by infiltrated tumor cells in the periphery of the radiation treatment regions, combinatorial strategies that induce an abscopal or bystander effect in patients will be critical for establishing local disease control and improving overall survival.

Funding

National Institute of Neurological Disorders and Stroke, National Institutes of Health (R25NS079200 to C.I.E.); National Cancer Institute, National Institutes of Health (U54CA193461-03, R01CA195718-02 to E.C.H.).

Acknowledgements

We would like to thank Jenny Zhang, Deby Kumasaka and James Yan of the Holland laboratory for their assistance. We would also like to thank Jamie Nguyen of the comparative medicine facility at the Fred Hutchinson Cancer Research Center for assistance with imaging including bioluminescence and MRI scans. We would also like to thank Kimberly Smythe of Experimental Histopathology, Fred Hutchinson Cancer Research Center.

References

1. Snuderl M, Fazlollahi L, Le LP, et al. Mosaic amplification of multiple receptor tyrosine kinase genes in glioblastoma. *Cancer Cell.* 2011;20(6):810-817.

2. Minniti G, Amelio D, Amichetti M, et al. Patterns of failure and comparison of different target volume delineations in patients with glioblastoma treated with conformal radiotherapy plus concomitant and adjuvant temozolomide. *Radiother Oncol.* 2010;97(3):377-381.

3. Mole RH. Whole body irradiation; radiobiology or medicine? *Br J Radiol.* 1953;26(305):234-241.

4. Crittenden M, Kohrt H, Levy R, et al. Current clinical trials testing combinations of immunotherapy and radiation. *Semin Radiat Oncol.* 2015;25(1):54-64.

5. D'Souza NM, Fang P, Logan J, Yang J, Jiang W, Li J. Combining Radiation Therapy with Immune Checkpoint Blockade for Central Nervous System Malignancies. *Front Oncol.* 2016;6:212.

6. Formenti SC, Rudqvist NP, Golden E, et al. Radiotherapy induces responses of lung cancer to CTLA-4 blockade. *Nat Med.* 2018;24(12):1845-1851.

7. Reardon DA, Kaley TJ, Dietrich J, et al. Phase II study to evaluate safety and efficacy of MEDI4736 (durvalumab) + radiotherapy in patients with newly diagnosed unmethylated MGMT glioblastoma (new unmeth GBM). *J Clin Oncol.* 2019;37:15(suppl):2032-2032.

8. Ahronian LG, Lewis BC. Using the RCAS-TVA system to model human cancer in mice. *Cold Spring Harb Protoc.* 2014;2014(11):1128-1135.

9. Hambardzumyan D, Amankulor NM, Helmy KY, Becher OJ, Holland EC. Modeling Adult Gliomas Using RCAS/t-va Technology. *Transl Oncol.* 2009;2(2):89-95.

10. Chen Z, Feng X, Herting CJ, et al. Cellular and Molecular Identity of Tumor-Associated Macrophages in Glioblastoma. *Cancer Res.* 2017;77(9):2266-2278.

11. Zhu H, Acquaviva J, Ramachandran P, et al. Oncogenic EGFR signaling cooperates with loss of tumor suppressor gene functions in gliomagenesis. *Proc Natl Acad Sci U S A.* 2009;106(8):2712-2716.

12. Holland EC, Hively WP, DePinho RA, Varmus HE. A constitutively active epidermal growth factor receptor cooperates with disruption of G1 cell-cycle arrest pathways to induce glioma-like lesions in mice. *Genes Dev.* 1998;12(23):3675-3685.

13. Mizutani M, Pino PA, Saederup N, Charo IF, Ransohoff RM, Cardona AE. The fractalkine receptor but not CCR2 is present on microglia from embryonic development throughout adulthood. *J Immunol.* 2012;188(1):29-36.

14. Morganti JM, Jopson TD, Liu S, Gupta N, Rosi S. Cranial irradiation alters the brain's microenvironment and permits CCR2+ macrophage infiltration. *PLoS One.* 2014;9(4):e93650.

15. Bloch O, Crane CA, Kaur R, Safaee M, Rutkowski MJ, Parsa AT. Gliomas promote immunosuppression through induction of B7-H1 expression in tumor-associated macrophages. *Clin Cancer Res.* 2013;19(12):3165-3175.

16. Gordon SR, Maute RL, Dulken BW, et al. PD-1 expression by tumour-associated macrophages inhibits phagocytosis and tumour immunity. *Nature.* 2017;545(7655):495-499.

17. Marconi R, Strolin S, Bossi G, Strigari L. A meta-analysis of the abscopal effect in preclinical models: Is the biologically effective dose a relevant physical trigger? *PLoS One.* 2017;12(2):e0171559.

18. Ngwa W, Irabor OC, Schoenfeld JD, Hesser J, Demaria S, Formenti SC. Using immunotherapy to boost the abscopal effect. *Nat Rev Cancer.* 2018;18(5):313-322.

19. Rutledge WC, Kong J, Gao J, et al. Tumor-infiltrating lymphocytes in glioblastoma are associated with specific genomic alterations and related to transcriptional class. *Clin Cancer Res.* 2013;19(18):4951-4960.

20. Wang R, Zhou T, Liu W, Zuo L. Molecular mechanism of bystander effects and related abscopal/cohort effects in cancer therapy. *Oncotarget.* 2018;9(26):18637-18647.

21. Verma V, Lin SH. Implications of the Bystander and Abscopal Effects of Radiation Therapy. *Clin Cancer Res.* 2016;22(19):4763-4765.

22. Huang Y, Lee C, Borgstrom P, Gjerset RA. Macrophage-mediated bystander effect triggered by tumor cell apoptosis. *Mol Ther.* 2007;15(3):524-533.

23. Hambardzumyan D, Gutmann DH, Kettenmann H. The role of microglia and macrophages in glioma maintenance and progression. *Nat Neurosci.* 2016;19(1):20-27.

24. Charles NA, Holland EC, Gilbertson R, Glass R, Kettenmann H. The brain tumor microenvironment. *Glia.* 2011;59(8):1169-1180.

25. Kerber M, Reiss Y, Wickersheim A, et al. Flt-1 signaling in macrophages promotes glioma growth in vivo. *Cancer Res.* 2008;68(18):7342-7351.

26. Watters JJ, Schartner JM, Badie B. Microglia function in brain tumors. *J Neurosci Res.* 2005;81(3):447-455.

27. Hartley GP, Chow L, Ammons DT, Wheat WH, Dow SW. Programmed Cell Death Ligand 1 (PD-L1) Signaling Regulates Macrophage Proliferation and Activation. *Cancer Immunol Res.* 2018;6(10):1260-1273.

28. Burrell K, Hill RP, Zadeh G. High-resolution in-vivo analysis of normal brain response to cranial irradiation. *PLoS One.* 2012;7(6):e38366.

29. Kleinovink JW, Marijt KA, Schoonderwoerd MJA, van Hall T, Ossendorp F, Fransen MF. PD-L1 expression on malignant cells is no prerequisite for checkpoint therapy. *Oncoimmunology.* 2017;6(4):e1294299.

Figure Legends

Figure 1. Combined unilateral radiation and systemic anti-PD-L1 immunotherapy increases survival in a bilateral glioblastoma model. (**A**) Strategy for inducing mouse bilateral glioblastoma within the brain using the RCAS/Tva mouse model for immune micro-environment profiling and Cre-recombination strategy used to generate unilateral luciferase expressing PDGF+Luc (top) and PDGF+EGFRvIII (bottom) tumors (Tg(NES-TVA);*Cdkn2a (Ink4a-Arf)*$^{-/-}$;*Pten*$^{fl/fl}$; LSL Luciferase and EGFRvIII mice). (**B**) Representative magnetic resonance imaging (MRI, left panel) of a bilateral glioblastoma mouse model. Right panel is bioluminescence signal from mouse in left panel, showing unilateral luciferase activity from the left-sided PDGF-*Pten*$^{-/-}$ tumor only. **Red arrows** delineate tumors on each side of brain. **Scale bar=**1mm. (**C**) Correlation between tumor viability (luciferase activity) and MRI T2-weighted signal in IgG-treated animals bearing bilateral glioblastoma (n=8 mice, R^2=0.9649). Two to three representative MRI scans highlighting interval growth in one untreated animal with arrows showing direction of growth between scans. **Red circles** are measurements from time point 1 (Post-tumor initiation day 17), **blue circles** are measurements from time point 2 (Post-tumor initiation day 20) and **green circles** are measurements from time point 3 (Post-tumor initiation day 23). Y-axis in logarithmic scale (Photons second^{-1}). X-axis in linear scale (mm^3). (**D-E**) Kaplan-Meier survival curves showing that anti-PD-L1 immunotherapy enhances unilateral radiation-induced survival in bilateral PDGF+Luc **(D)** and PDGF+EGFRvIII **(E)** glioblastoma (n=6-8 mice per treatment group). **Red arrow** indicates unilateral 10Gy irradiation. **Blue arrow** indicates daily anti-PD-L1 or anti-PD-1 treatments. Treatments began on post-tumor initiation day 15. Log-rank Mantel–Cox test for radiation alone versus radiation with anti-PD-L1. P <.05-* for PDGF+Luc, P <.01- ** for PDGF+EGFRvIII.

Figure 2. Abscopal effect of combined localized radiation and systemic anti-PD-L1 immunotherapy. (**A**) Depiction of experimental strategy of bilateral mouse glioblastoma to measure abscopal effect in Tg(*NTva*);*Ink4a-Arf*$^{-/-}$;*Pten*$^{-/-}$; LSL Luciferase mice with left-sided PDGF-*Pten*$^{-/-}$ Luciferase tumor and right-sided PDGF-shPten tumor. The right hemisphere contains a non-luciferase tumor and is radiated. The left side contains neoplastic cells harboring luciferase expression and is not radiated. Tumor viability (Photons seconds^{-1}) and MRI tumor volume (mm^3) are obtained from the left-sided, non-radiated tumor only. (**B**) Association between tumor viability (Photons seconds^{-1}) and MRI tumor volume (mm^3) for all treatment groups. The growth pattern of each individual animal is shown as black lines and the linear regression summation of all the animals in the treatment group are depicted as colored wide arrows. Mice receiving combination imaging included IgG control (n=8, red), whole brain radiation (n=4, purple), non-luciferase tumor radiation alone (n=4, magenta), anti-PD-L1 alone (n=4, blue) and non-luciferase tumor radiation with anti-PD-L1 (n=8, green). Tumor viability (luciferase activity in photons second^{-1}) and MRI T2 signal volume (mm^3) is shown relative to pre-treatment starting point that was normalized to 100% for all mice. (**C**) Response of un-irradiated tumor to treatment is categorized as transient tumor regression (TTR) or sustained tumor regression (STR). TTR represents any decrease in un-irradiated tumor viability (luciferase activity) that is followed by un-irradiated tumor re-growth. STR represents any decrease in un-irradiated tumor viability that is not followed by un-irradiated tumor re-growth prior to reaching endpoint. Relative to IgG treated animals (red), whole brain radiation (10Gy) or radiation positive control induces TTR in 7 of 7 mice with STR in 0 of 7 mice. Anti-PD-L1 antibody alone does not induce TTR or STR in any mice (0 of 7 mice). Unilateral radiation of non-luciferase expressing tumor induces TTR in 2 of 7 mice with STR in 0 of 7 mice. Unilateral radiation of non-luciferase tumor and anti-PD-L1 antibodies induces TTR in 6 of 8 mice with STR in 2 of 8 mice. All post-treatment viability is shown relative to the original tumor

viability, with growth showing increase and treatment response showing decrease on a $\log_{10}$ scale. IgG isotype control is the same for all treatment groups and **shown in red**, relative to experimental group **shown in blue**.

Figure 3. Localized radiation and systemic anti-PD-L1 immunotherapy promotes intra-tumoral macrophage and T-cell infiltration. (A-B). Quantification of $Iba1^+$ macrophage influx into un-irradiated or abscopal side **(A)** and radiated side **(B)** based on immunohistochemistry on PDGF+Luc (red) and PDGF+EGFRvIII (blue) mouse gliomas on post-treatment day 10, n=5 mice per group. **(C-D).** Quantification of $CD3^+$ T-cells macrophage influx into un-irradiated or abscopal side **(C)** and radiated side **(D)** based on immunohistochemistry on PDGF+Luc (red) and PDGF+EGFRvIII (blue) mouse gliomas following treatment, n=5 mice per group. **(E-F)** Representative immunohistochemistry for macrophages (Iba1) in PDGF+Luc gliomas **(E)** and T-cells (CD3) in PDGF+EGFRvIII gliomas **(F)** following treatment (Abscopal side). 3-5 high powered fields were counted per tumor sample from 5 different tumors on post-treatment day 10. **Scale bar**=50μm. P-values derived from the non-parametric Mann-Whitney U test, two-sided. Holm-Bonferroni multiple comparison post hoc test for **A-D**. **Error bars**=SEM. P <.05- *, P <.01- **, P <.001-***, P<.0001-****, NS=not significant.

Figure 4. T-cell depletion does not affect abscopal effect in PDGF+Luc glioblastoma

(**A-B**) Bioluminescence **(A)** and survival data **(B)** from Tg(*NTva*);*Ink4a-Arf*$^{-/-}$;*Pten*$^{-/-}$; LSL Luciferase mice with left-sided PDGF-*Pten*$^{-/-}$ Luciferase tumor and right-sided PDGF-shPten tumor treated with anti-mouse IgG_2b isotype control (n=7), anti-CD8 (n=8) and anti-CD4 (n=8) depleting antibodies at 10, 15, 19, 22 and 30 days post-tumor initiation (**black arrows** in **B**). Unilateral 10Gy radiation was then administered (**red arrow** in **B**) followed by daily anti-PD-L1 therapy. Based on luciferase activity

measured within 10 days post-treatment initiation, abscopal response seen in 7/7 IgG treated mice, 8/8 $CD8^+$ T-cell depleted mice and 8/8 $CD4^+$ T-cell depleted mice. Survival curves following T-cell depletion in radiation and anti-PD-L1 treated mice showing no impact of T-cell depletion on survival (**B**). Log-rank Mantel–Cox test for radiation alone versus radiation with anti-PD-L1. P <.01- **, NS=not significant. (**C**) To verify T-cell depletion, flow cytometry was performed on spleens harvested from combination therapy treated mice (n=2 per group) on post-tumor initiation day 22 after 2 doses of depleting antibodies demonstrating >90% depletion. (**D** and **E**) On post-treatment day 5, relative to radiation alone (n=6, red), combination therapy with anti-PD-L1 immunotherapy (n=6, blue) is associated with increased infiltration of bone marrow derived macrophages ($CX3CR1^{+/GFP}$/$CCR2^{+/RFP}$) into the non-radiated/abscopal side as shown in **D**, and radiated side as shown in **E**, of bilateral RCAS-PDGF-driven glioblastoma in *Ntva; Cdkn2a^{wt}; Pten$^{flox/flox}$; CX3CR1$^{+/GFP}$; CCR2$^{+/RFP}$* mice. **Red circles** are unilateral radiation treated mice, **blue squares** are unilateral radiation and anti-PDL1 treated mice. P-values derived from the non-parametric Mann-Whitney U test, two-sided. **Error bars**=SEM. P <.01- **, NS=not significant.

Figure 5. Anti-PD-L1 antibodies directly activate bone marrow derived macrophages.

(**A** and **B**) Gene ontology analysis of differentially expressed genes following incubation of anti-PD-L1 antibodies with macrophages *in vitro*. Cell signaling pathways are shown in **A** and cell cycle/cytokine activation shown in **B**. We noted both activating and inhibitory signaling following anti-PD-L1 treatment of macrophages in-vitro (**Red** – upregulation; **Blue** – downregulation). Gene expression is based on average fold-change from mouse bone marrow derived macrophages from three different mice pools. (**C**-**F**) Anti-PD-L1 antibodies induces ERK phosphorylation (p44/42) in mouse bone marrow derived macrophages, quantified in **D** and human peripheral blood monocyte derived macrophages,

quantified in **E** and **F**. Lysates were collected at 30 minutes and 3 hours post-treatment with anti-PD-L1 antibodies. Two clinical grade human monoclonal antibodies (mAb) were evaluated including Avelumab (Bavencio, Merck, Kenilworth, New Jersey) and Atezolizumab (Tecentriq, Genentech, San Francisco, California). Selective ERK inhibition with PD98059 (Cell Signaling) is shown in a dose dependent manner. Matched isotype antibody was used as a negative control. Total ERK is the loading control. Results were independently replicated in different mouse bone marrow derived macrophages derived from three different mice pools and two different healthy human peripheral blood mononuclear cells donors.

Figure 6. Anti-PD-L1 enhances macrophage phagocytosis in PDGF+Luc gliomas

(**A**) Anti-PD-L1 antibodies promote phagocytosis of FITC-labelled *E.coli* particles *in vitro* via ERK signaling in PD-L1^{+}/PD-1^{-} murine macrophages. Phagocytosis of the particles was measured by a Vybrant phagocytosis assay kit. This anti-PD-L1 effect on macrophages is inhibited by PD98059, an ERK inhibitor (20μM). Three biological replicates each, with three technical replicates are shown. **Orange** are IgG controls, **pink** are FcγR (CD16/32) receptor block, **blue** are anti-PD-L1 without ERK inhibitor, **red** are anti-PD-L1 with ERK inhibitor, **green** are anti-PD-1 without ERK inhibitor, **black** are anti-PD-L1 with ERK inhibitor (**B**) Percent phagocytosis represents the proportion of Iba1^{+} cells (macrophages) that have circumferentially encircled an Olig2^{+} neoplastic cell. Counts from at least five high powered fields (40x objective) per animal from post-treatment day 10. Each point represents a single animal with bilateral tumors from PDGF+Luc glioblastoma (n=5-6 mice per treatment group). **Orange** are IgG control, **pink** are unilateral radiation only, **blue** are irradiated side of anti-PD-L1 with unilateral radiation, **red** are abscopal side of anti-PD-L1 with unilateral radiation (**C**) Representative immunofluorescence microscopy for Hoechst (all nuclei), Olig2 (neoplastic cells) and Iba1

(macrophages) in PDGF+Luc (radiated side) mouse glioblastoma on post-treatment day 10. Yellow arrows indicate phagocytosed Olig2^{+} neoplastic cells (Magnification, 40x; **Scale bar**=30μm). P-values derived from the non-parametric Mann-Whitney U test, two-sided. **Error bars**=SEM. P <.01- **, P<.0001-****, NS=not significant.

Figure 1

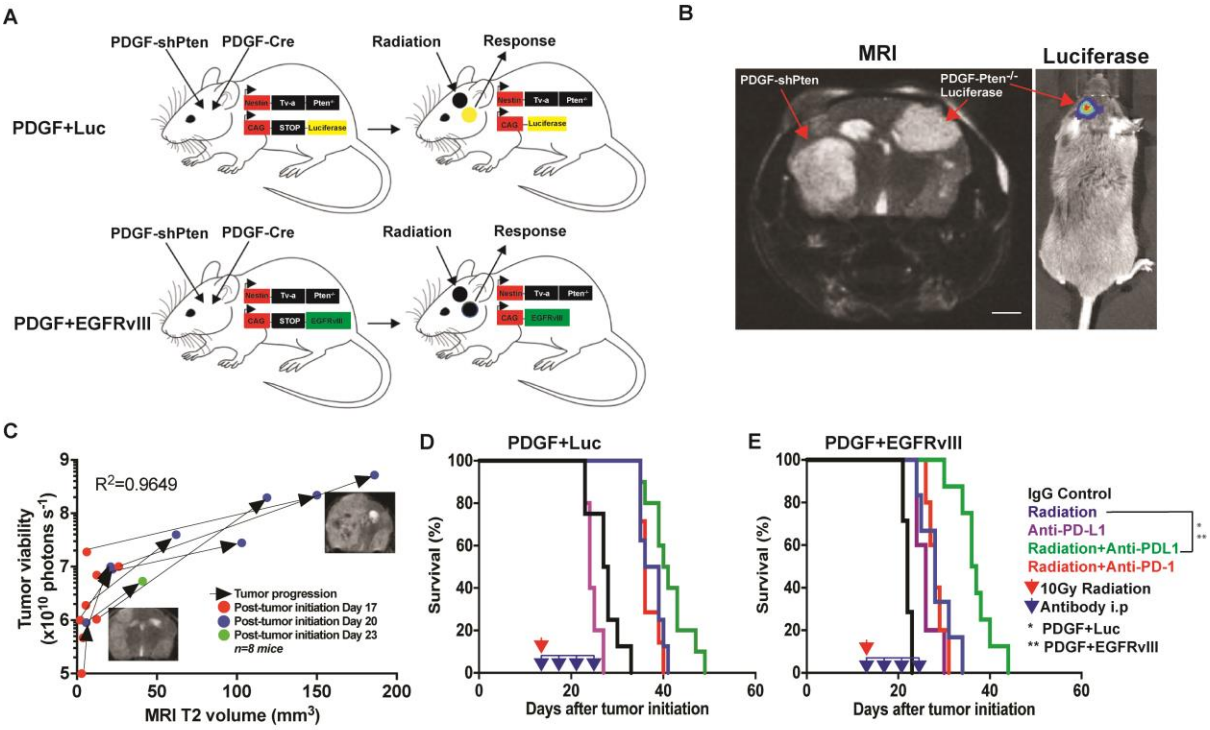
A
PDGF-shPten
PDGF-Cre
Radiation
Response
PDGF+Luc
PDGF+EGFRvIII
B
MRI
Luciferase
PDGF-shPten
PDGF-Pten-/-
Luciferase
C
R2=0.9649
Tumor viability
(x10^10 photons s-1)
MRI T2 volume (mm3)
Tumor progression
Post-tumor initiation Day 17
Post-tumor initiation Day 20
Post-tumor initiation Day 23
n=8 mice
D
PDGF+Luc
Survival (%)
Days after tumor initiation
E
PDGF+EGFRvIII
Survival (%)
Days after tumor initiation
IgG Control
Radiation
Anti-PD-L1
Radiation+Anti-PDL1
Radiation+Anti-PD-1
10Gy Radiation
Antibody i.p
* PDGF+Luc
** PDGF+EGFRvIII

Figure 2

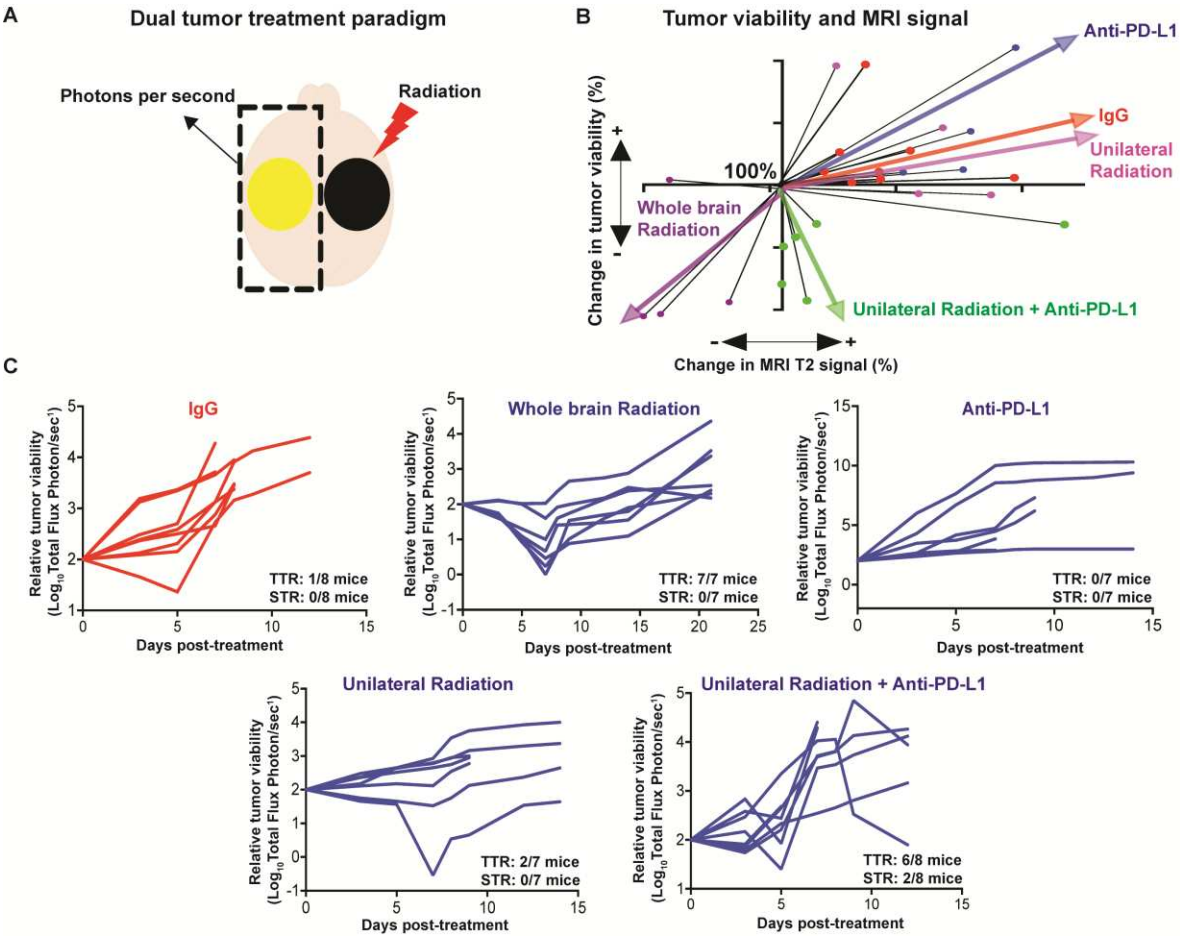
A
Dual tumor treatment paradigm
Photons per second
Radiation
B
Tumor viability and MRI signal
Anti-PD-L1
IgG
Unilateral Radiation
100%
Whole brain Radiation
Unilateral Radiation + Anti-PD-L1
Change in tumor viability (%)
Change in MRI T2 signal (%)
C
IgG
TTR: 1/8 mice
STR: 0/8 mice
Whole brain Radiation
TTR: 7/7 mice
STR: 0/7 mice
Anti-PD-L1
TTR: 0/7 mice
STR: 0/7 mice
Unilateral Radiation
TTR: 2/7 mice
STR: 0/7 mice
Unilateral Radiation + Anti-PD-L1
TTR: 6/8 mice
STR: 2/8 mice
Relative tumor viability (Log10 Total Flux Photon/sec-1)
Days post-treatment

Figure 3

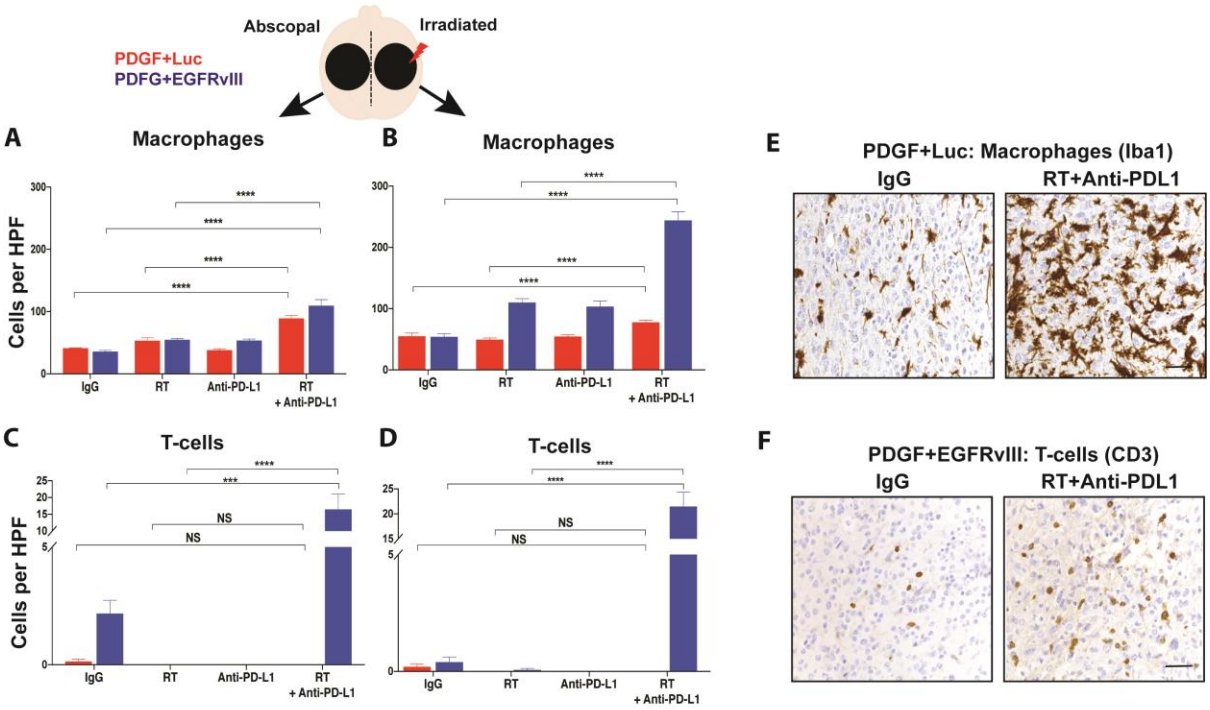
Abscopal
Irradiated
PDGF+Luc
PDFG+EGFRvIII
A
Macrophages
B
Macrophages
Cells per HPF
IgG
RT
Anti-PD-L1
RT + Anti-PD-L1
C
T-cells
D
T-cells
NS
E
PDGF+Luc: Macrophages (Iba1)
IgG
RT+Anti-PDL1
F
PDGF+EGFRvIII: T-cells (CD3)
IgG
RT+Anti-PDL1

Figure 4

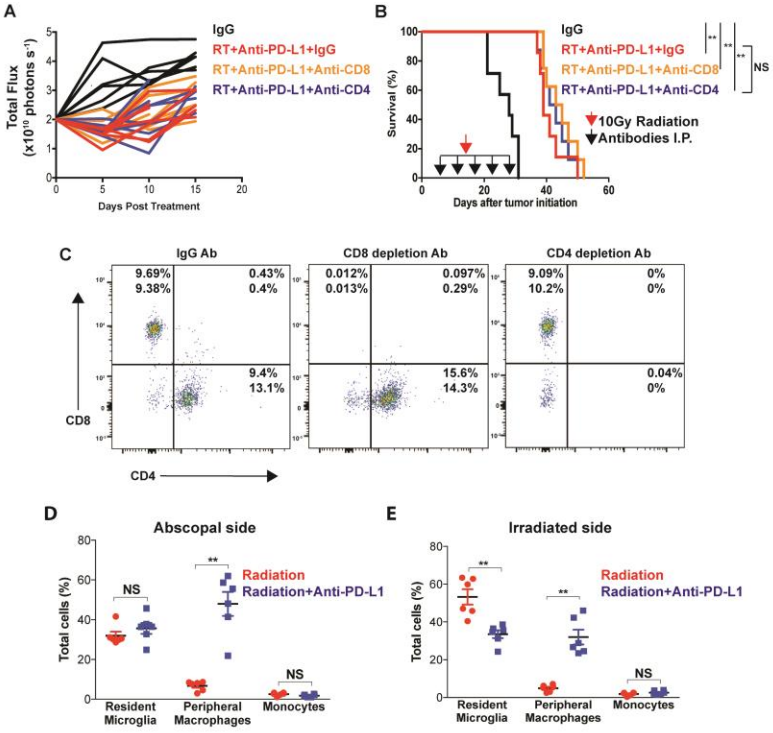
A
Total Flux (x10^10 photons s^-1)
Days Post Treatment
IgG
RT+Anti-PD-L1+IgG
RT+Anti-PD-L1+Anti-CD8
RT+Anti-PD-L1+Anti-CD4
B
Survival (%)
Days after tumor initiation
10Gy Radiation
Antibodies I.P.
**
**
**
NS
C
IgG Ab
CD8 depletion Ab
CD4 depletion Ab
9.69%
9.38%
0.43%
0.4%
9.4%
13.1%
0.012%
0.013%
0.097%
0.29%
15.6%
14.3%
9.09%
10.2%
0%
0%
0.04%
0%
CD8
CD4
D
Abscopal side
Total cells (%)
Radiation
Radiation+Anti-PD-L1
NS
**
NS
Resident Microglia
Peripheral Macrophages
Monocytes
E
Irradiated side
Total cells (%)
Radiation
Radiation+Anti-PD-L1
**
**
NS
Resident Microglia
Peripheral Macrophages
Monocytes

Figure 5

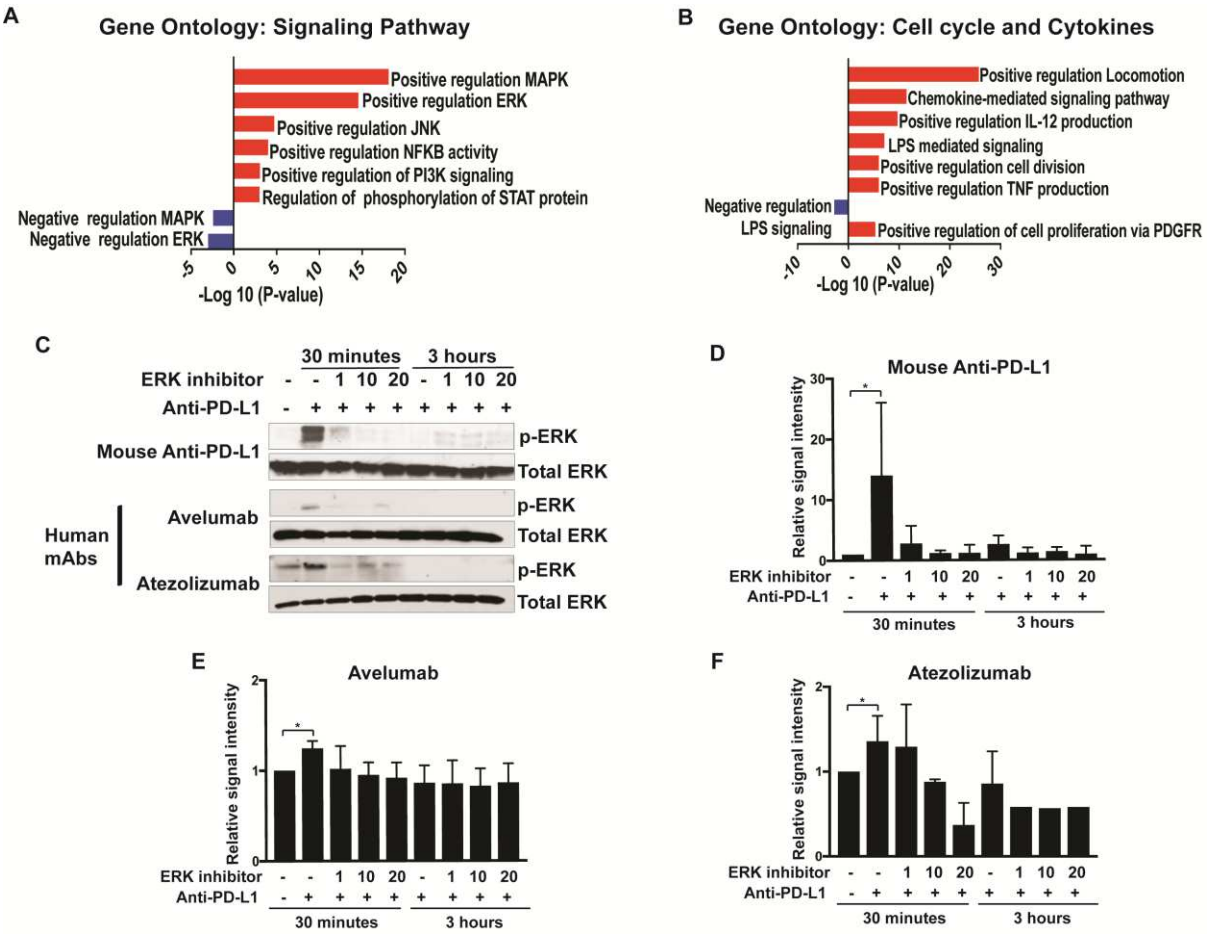
A
Gene Ontology: Signaling Pathway
Positive regulation MAPK
Positive regulation ERK
Positive regulation JNK
Positive regulation NFKB activity
Positive regulation of PI3K signaling
Regulation of phosphorylation of STAT protein
Negative regulation MAPK
Negative regulation ERK
-5 0 5 10 15 20
-Log 10 (P-value)
B
Gene Ontology: Cell cycle and Cytokines
Positive regulation Locomotion
Chemokine-mediated signaling pathway
Positive regulation IL-12 production
LPS mediated signaling
Positive regulation cell division
Positive regulation TNF production
Negative regulation LPS signaling
Positive regulation of cell proliferation via PDGFR
-10 0 10 20 30
-Log 10 (P-value)
C
30 minutes
3 hours
ERK inhibitor - - 1 10 20 - 1 10 20
Anti-PD-L1 - + + + + + + + +
Mouse Anti-PD-L1
p-ERK
Total ERK
Human mAbs
Avelumab
p-ERK
Total ERK
Atezolizumab
p-ERK
Total ERK
D
Mouse Anti-PD-L1
Relative signal intensity
0 10 20 30
*
ERK inhibitor - - 1 10 20 - 1 10 20
Anti-PD-L1 - + + + + + + + +
30 minutes
3 hours
E
Avelumab
Relative signal intensity
0 1 2
*
ERK inhibitor - - 1 10 20 - 1 10 20
Anti-PD-L1 - + + + + + + + +
30 minutes
3 hours
F
Atezolizumab
Relative signal intensity
0 1 2
*
ERK inhibitor - - 1 10 20 - 1 10 20
Anti-PD-L1 - + + + + + + + +
30 minutes
3 hours

Figure 6

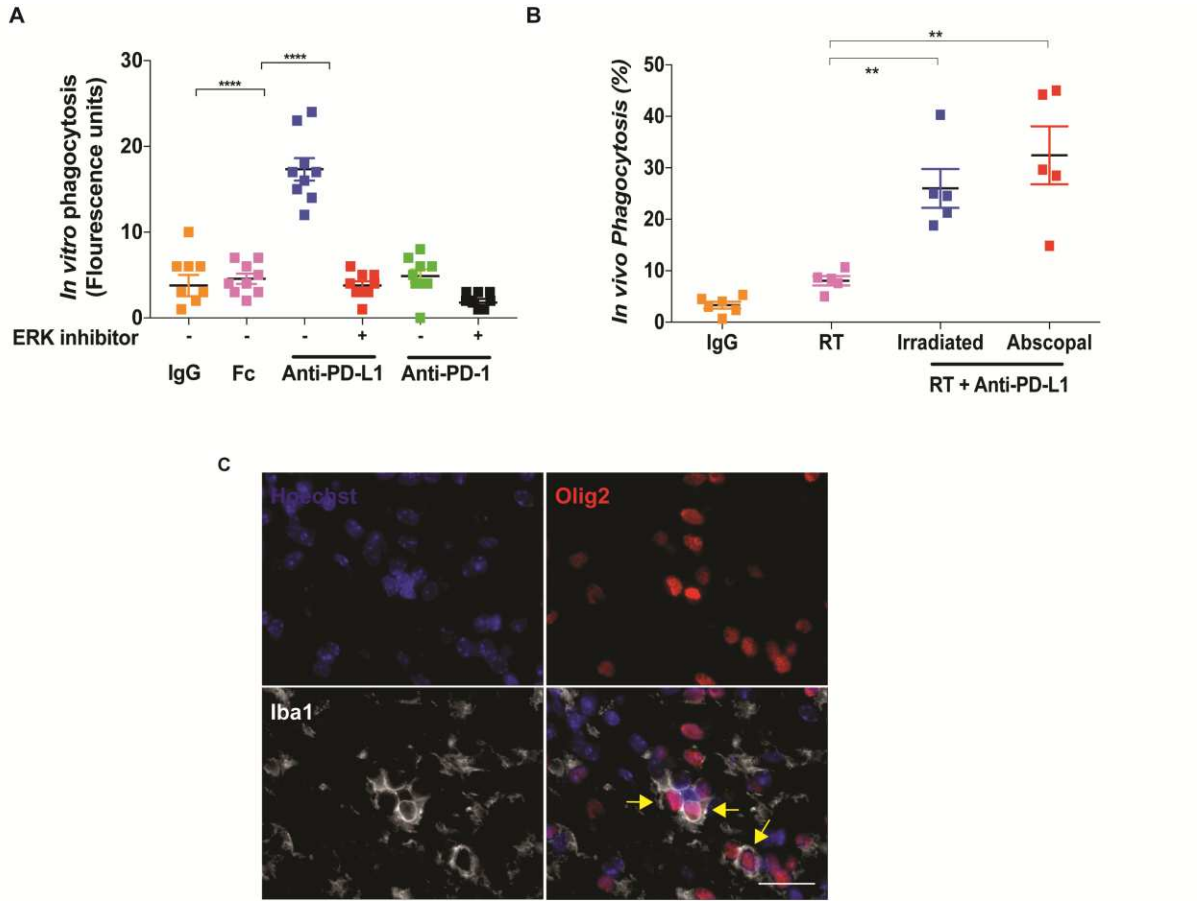
A
In vitro phagocytosis (Flourescence units)
30
20
10
0
****
****
ERK inhibitor
-
-
-
+
-
+
IgG
Fc
Anti-PD-L1
Anti-PD-1
B
In vivo Phagocytosis (%)
50
40
30
20
10
0
**
**
IgG
RT
Irradiated
Abscopal
RT + Anti-PD-L1
C
Hoechst
Olig2
Iba1